DETECTION OF RADIOACTIVE SEEDS IN ULTRASOUND IMAGES OF THE PROSTATE

Yongjian Yu[1], *Scott T. Acton*[1] *and Ken Thornton*[2]

[1] Department of Electrical and Computer Engineering, University of Virginia, Charlottesville, VA 22904
[2] Varian Medical Systems, Charlottesville, VA 22901

ABSTRACT

This paper presents a robust technique for automatically detecting radioactive seeds that are used for prostate cancer therapy. The main innovation of the detection technique is the utilization of distributed constant false alarm rate (CFAR) processors and orientation-sensitive morphological filtering to locate the seeds in the ultrasound imagery. CFAR detection is utilized to detect the seed candidates with high signal-to-clutter ratios (SCR's). The CFAR problem is posed as the detection of a fluctuating target against K-distributed clutter. Adaptive template matching is used to detect the weak seed signals and to discriminate the seed-like clutter from the seed candidates. To reduce the speckle noise, the adaptive template matching uses orientation-sensitive morphological filters. The complete detection algorithm has been tested using a set of phantom ultrasound images containing radioactive seeds. In the process of implantation of seeds for radiotherapy, the detection method can be used to evaluate seed placement before 3-D reconstruction is accomplished.

1. INTRODUCTION

Cancer of the prostate is reported to be the second most frequently diagnosed cancer in the United States male population and is the third most frequent cause of cancer death [1]. Recently, percutaneous transperinal implant of radioactive seeds has been utilized with success for the treatment of prostatic carcinoma [1]. This treatment is fast becoming a preferred alternative to standard treatments involving the surgical removal of the prostate gland or repeated external-beam radiation therapy.

Ultrasound, a commonly used medical imaging modality with numerous other medical applications such as demonstrating blood flow through a vessel, estimating the extent of prostatic cancer, and assessing the health of the fetus, has been used as a guide for the radiation treatment and planning for cases that involve prostatic carcinoma. In the ultrasound guided radioactive seed implantation, the seed detection, recognition and precision positioning are essential in achieving the best curative effects within the targeted zones, at the lowest cost of damaging neighboring healthy tissues or organs. Although ultrasound imaging has several benefits including the low cost, the real-time imaging ability and the absence of dangerous radiation, the ultrasound imagery suffers from degradation that renders the interpretation by humans cumbersome. In our application, we desire an automated seed detection process that will be used in implantation before the 3-D reconstruction is computed.

This work studies the usefulness and robustness of the constant false alarm rate (CFAR) detection and adaptive template matching in the detection of radioactive seeds in ultrasound imagery (see Figure 1). After a general description of the algorithm is presented in section 2.1, the CFAR detectors for seed detection in the K-distributed clutter are formulated in section 2.2. Theoretical detection performance is also presented in this section for the design of actual detectors in our experiments. Next, the adaptive template matching is addressed in section 2.3, focusing on template extraction. Finally, experimental results and conclusions are provided that demonstrate the efficacy of the approach.

2. DETECTION ALGORITHM

2.1. General description of the detection algorithm

The overall detection algorithm consists of two parts: (1) the distributed CFAR detection and (2) adaptive template matching. With the properly designed CFAR detection scheme, the set of seed candidates including the strong seed signals, weak seed signals and seed-like clutter can be detected. Complementary to CFAR detection, the adaptive template matching is used to detect weaker seeds that are neglected by one of individual CFAR processors and to eliminate the seed-like clutter that produces false detections. To make better use of the geometry of the ultrasound imagery, a polar coordinate system is adopted. The origin of the system is located at the imaging transducer and the line of sight of the transducer is in the axial direction.

The distributed CFAR detection is completed in two steps. Firstly, two subsets of seed candidates are detected by applying axial and lateral CFAR detectors. Secondly, a fusion criterion is used to merge those seed candidates, yielding the set of strong seed signals and forming a complete set of seed candidates.

The template matching proceeds as follows. Firstly, the central positions of the strong seed signals are estimated. Then, a typical seed template is extracted from the sub-images of the detected bright seeds. Next, the template and the sub-images of all seed candidates, except for those detected as strong seed signals, are preprocessed with orientation-sensitive image morphology. Finally, a cross-correlation algorithm is applied to recover the weak seeds and remove seed-like clutter.

The central problem in the CFAR solution is posed as detecting fluctuating target against K-distributed clutter. A spatially rotating seed template manifests the adaptivity of the template matching.

0-7803-6725-1/01/$10.00 ©2001 IEEE

2.2. Distributed CFAR detection

In this section, we first present and justify the choice of the models for the clutter and for the target seeds. Based on these models, we then proceed to formulate the detection and false alarm probabilities for cell average (CA) and order statistic (OS) detectors followed by a description of individual processors. Lastly, we present the fusion criterion.

2.2.1.Clutter and Target-plus-clutter statistical models

As with coherent radar imagery, pulse-echo ultrasound imagery are heavily affected by speckle noise that results from the random scatter produced by reflecting scatterers that have dimensions of the same scale as the sound wavelength. In the imagery of blood cells, the fluctuations of a speckle pattern exhibit Rayleigh-distributed amplitude with standard deviation equal to the mean. This kind of speckle pattern is fully developed and ideal; however, the pattern occurs only when many fine randomly distributed scattering elements exist within the resolution cell of the imaging system. More generally, tissue scatter may be better modeled as having a multiplicative, signal-dependent K distribution. This kind of scatter contributes a coherent or specular backscattered intensity that is itself spatially variant. Another class occurs when a spatially invariant coherent structure is present within the random scatterer region such as organ surfaces and blood vessels. The probability density function of the echo signals becomes Rician distributed in this case [2].

Recent histological studies [1] have shown that the prostate is divided into two major zones: the prostatic glandular zone and the periurethral zone. The glandular prostate is separated into a peripheral and a central zone of acinar tissue. The central zone is composed of irregular, large acini. Parts of prostatic urethra and the ejaculatory ducts and the verumontanum are collocated. The acini of the peripheral zone are smaller and rounder with smooth walls and are more uniform in size. The muscular stroma is also a different tissue found in the area. The central zone's stroma is compactly arranged. But the musculature of the peripheral zone is more random and not as tightly interwoven.

Hence, we know that the detection of seed is to be carried out in a complex clutter environment. Therefore, the prostate clutter envelope may be better approximated by the K-distribution. The amplitude probably density function for pure clutter in a non-coherent integrated data set is assumed to be

$$f_{X_0}(x) = \frac{4c}{\Gamma(\nu)\Gamma(L)}(cx)^{\nu+L-1} K_{\nu-L}(2cx) \tag{1}$$

where L is the effective number of looks for the non-coherent integrated image data, ν is the shape parameter, c is a power parameter such that $P_0 = (L \cdot \nu)/c^2$ is the clutter average power, and $K_\nu(x)$ the modified Bessel function of the second kind.

In the target-plus-clutter region, if we assume the amplitude of the pure target adheres to a gamma distribution of $2L$ degrees of freedom, then we can compute the overall amplitude PDF of the target-plus-clutter random variable X, *i.e.*,

$$f_{X_1}(x) = \int_0^\infty p(u) \cdot f_{X_1|u}(x)du, \tag{2}$$

where the conditional PDF $f_{X_1|u}(x)$ is given by

$$f_{X_1|u}(x) = \frac{2}{\Gamma(L)}\left(\frac{L}{4u^2/\pi + 2\sigma_t^2}\right)^L \cdot x^{2L-1} \cdot \exp\left(-\frac{Lx^2}{4u^2/\pi + 2\sigma_t^2}\right),$$

while $p(u) = \frac{2b^{2\nu}}{\Gamma(\nu)} \cdot u^{2\nu-1} \cdot \exp(-b^2u^2)$ with $b = c\sqrt{4/\pi}$, and $2\sigma_t^2$ is the target mean power.

2.2.2. CA- and OS- CFAR processors

Given the PDF of the test statistic Z, $p_Z(z)$, for a specific CFAR technique, the false alarm probability is given by

$$\begin{aligned} P_{fa} &= E_Z\{P[X_0 > Tz \mid H_0]\} \\ &= \int_0^\infty P[X_0 > Tz \mid H_0] \cdot p_Z(z)dz \end{aligned} \tag{3}$$

where $P[X_0 > Tz \mid H_0]$ is the complementary cumulative distribution function (CCDF) of the clutter PDF at threshold Tz,

$$\begin{aligned} P[X_0 > Tz \mid H_0] &= \int_{Tz} f_{X_0}(x)dx \\ &= \frac{2}{\Gamma(\nu)}\sum_{m=0}^{L-1}\frac{1}{\Gamma(L-m)}(cTz)^{\nu+L-m-1} K_{\nu-L+1+m}(2cTz) \end{aligned} \tag{4}$$

where T is a threshold multiplier factor.

Assuming that a target has a signal-to-clutter ratio (SCR) of R ($R \equiv 2\sigma_t^2/(L\nu/c^2)$), the detection probability of the target can be expressed as

$$P_D = E_Z\{P[X_1 > Tz \mid H_1]\} \tag{5}$$

where $P[X_1 > Tz \mid H_1] = \int_0^\infty p(u) \cdot P_{Y|u}(y > Tz)du$ and

$$\begin{aligned} P_{Y|u}(y > Tz) &= \int_{Tz}^\infty f_{X_1|u}(x)dx \\ &= \exp\left[-\frac{L(Tz)^2}{4u^2/\pi + RL\nu/c^2}\right] \cdot \sum_{m=0}^{L-1}\frac{1}{m!}\left[\frac{L(Tz)^2}{4u^2/\pi + RL\nu/c^2}\right]^m. \end{aligned}$$

The CFAR technique is accomplished by collecting N reference samples and implementing the adaptive threshold test:

$$X \underset{H_0}{\overset{H_1}{\gtrless}} TZ. \tag{6}$$

where H_0 is null hypothesis, H_1 is target existing hypothesis.

In the cell average (CA) CFAR processor, the test statistic Z is taken as the sum of the amplitudes of N referenced samples:

$$Z = \sum_{i=1}^{N} X_i.$$

The test statistic for the order statistic (OS) CFAR processor is taken as the amplitude of the k^{th} ranked pixel among the N referenced pixels in ascending order in accordance with their intensity magnitudes: $Z = X^{(k)}$.

If we assume that the observations in the reference window are statistically independent and identically distributed (IID), then the PDF's of the test statistic of the local clutter Z are

$$p_Z^{CA}(z) = \underbrace{f_{X_0}(z) * f_{X_0}(z) * \ldots * f_{X_0}(z)}_{N-fold\ convolution}, \tag{7}$$

$$p_Z^{OS}(z) = k\binom{N}{k} \cdot [1 - P(z)]^{N-k} \cdot [P(z)]^{k-1} \cdot f_{X_0}(z), \tag{8}$$

where $P(z)$ is the CDF of the of the clutter.

By substituting the $p_Z^{CA}(z)$ or $p_Z^{OS}(z)$ into (4) and (5), we can design our CFAR processors, compute the corresponding T for a constant P_{fa} and SCR for a specific P_D.

As an illustration, (2) - (5) are used to evaluate theoretical detection performance for certain CFAR CA and OS. Figure 1 shows the plots of the probabilities of detection and false alarm vs. threshold multiplier factor for a (a) CA processor with N=6, L=16, SCR=10dB and v=1.5; (b) for OS processor with N=6, L=16, k=2, SCR=10dB, and v=1.5.

2.2.3.Structures of individual CFAR processors

By observing the B-mode ultrasound imagery of the phantom prostate as shown in Figure 1, we find that the seed signals have geometrical symmetry with respect to the line of sight of the imaging system. Moreover, the effective field of view lies only in a sector.

To take full advantage of the geometrical features of the seed and the effective sector of the image, the first CFAR processor is applied to a number of subregions (with one end at the position of the transducer) scanning across the effective image sector. One such subregion is illustrated in Figure 3 (a). Instead of applying the CFA processor to the full resolution image, we apply the processor to a preprocessed low-resolution image with such a scale that individual seeds appear as point targets. Through a combination of filtering and subsampling, we can create any desired high-scale representation of the base image.

With this processor, a constant threshold coefficient can be set for all subregions for a required probability of false alarm (P_{fa}) value.

We then apply another CFAR processor to a number of lateral subregions spanning over the effective image sector, one of which is shown in Fig.3 (b). Similarly, we apply the CFAR processor to a preprocessed low-resolution image.

2.2.4. Detection fusion

At the fusion stage, the detection problem is posed as a hypothesis test in which:

$$\begin{aligned} &\textit{Strong seed hypothesis } K_1 : S_1 = S_2 = S^* \\ &\textit{Seed candidate hypothesis } K_0 : S_i = S^* \quad i = 1,2 \end{aligned} \tag{9}$$

where S_i is the detection decision at the i^{th} processor. The symbol $=$ denotes that at least one of the S_i decisions is equal to S^*, where the symbol S^* represents the H_1 decision in the individual CFAR processor.

The fusion rule for K_1 is AND, which decides in favor of K_1 only if both processors detect a seed. Since the individual CFAR processors detect stronger seed signals with higher probability, this fusion rule yields the brightest seeds with the high confidence. The OR rule in the fusion stage detects the complete set of seed candidates by union of two subsets of seed candidates.

2.2.5. Distribution parameter estimation

To design the CFAR processors, the K distribution order parameter ν for clutter needs to be selected. The order parameter may be estimated by [3]

$$(1+1/L)(1+1/\nu) = \langle t \rangle, \tag{10}$$

where $\langle t \rangle$ is the average of the normalized intensity square over a uniform region, $t = I^2/\langle I \rangle^2$, I is intensity image. However, this estimator is appropriate only when the value of ν is large.

It has been established that the order parameter can be estimated for low order values by solving [4]

$$\mathrm{var}[\ln(I)] = \psi'(\nu) + \psi'(L), \tag{11}$$

where $\psi'(x)$ is the derivative of the digamma function $\psi(x)$, and var[ ] is the variance of the logarithmic of the intensity image over a uniform clutter region.

As a compromise, (10) is first used to find an initial estimate of ν. If this initial value is high (>5), the estimate is accepted; otherwise (11) is used to refine the estimate. Estimated values of the clutter order parameter may vary in a wide range. Using our experimental data, a range of 1.5 to 16 has been observed.

2.3. Adaptive template matching

In this section, we address enhancement of the detection performance through the use of an adaptive template matching technique. We utilize the seed patterns from the high SCR cases to form templates that locate the weaker seed signals.

To achieve seed position estimation, we employ a p-tile threshold that selects the corresponding right tail of the histogram of the prefiltered sub-image of typical bright seed. Then, to preserve the shape of the seed signal, we use orientation-sensitive morphological filters (open filters) in each sub-image containing candidate seeds. The structuring element has a rectangular shape, but is adaptively tilted such that it is in alignment with the line of sight passing the center of the window. Fig. 4 shows a comparison of the filtered images with conventional opening and an orientation-sensitive morphological filter. An improvement in preserving details is observed with the adaptive filter.

After enhancement, the set of seed candidates and seed-like clutter signatures as well as the strong seed signals have been detected and identified. Here, we try to recover weak seed signals and remove the remaining clutter. To do so, we use the detected seed images to form a sequence of adaptive template images, and apply the templates on the sites of all seed candidate positions to detect additional seeds.

Because the seed is a 3-D target, the last step in the detection algorithm is the seed center estimation. This step is structured simply as a seed sub-image centroid computation. The sub-image is also taken as a tilted rectangle using the same window as the structuring element applied in the orientation-sensitive morphological filer.

3. EXPERIMENTS AND RESULTS

The proposed algorithm has been tested to detect seeds using 5-MHz ultrasound sector B-scan imagery of a prostate phantom, as shown in Fig.2. Shaped like a flattened cone, an average-sized normal prostate measures approximately 4 cm in

maximum transverse diameter, 3 cm in anterior-posterior dimension, and 3.8 cm in cephalocaudad projection.

Fig. 5 shows the detection results with an 'X' marking each detected seed. Table I shows real performance of the detection algorithm obtained with ground truth validation. Here MAE indicates the maximum absolute error (in millimeter) of seed positioning. In general, we achieve a correct detection rate of 93.7%, a false alarm rate of 8.7% and a miss rate is 6.2%. This verifies the effectiveness of our algorithm, which allows precision analysis of the seed implantation process used to combat prostate cancer.

4. REFERENCES

[1] Matthew D. Rifkin, *Ultrasound of the Prostate*, Raven Press, 1988.

[2] Khaled Z. Abd-Elmoniem, Yasser M. Kadah, and Abou-Bakr M. Youssef, "Real Time Adaptive Ultrasound Speckle Reductoin And Coherence Enhancement," *ICIP 2000 proceedings*, Vancouver, Canada, pp. 1106-1109, 2000.

[3] J.S. Lee, D.L. Schuler, R. H. Lang, K. J. Ranson., "K-distribution for multi-look processed polarimetric SAR imagery," *IGARSS'94*, vol. 4, pp.2179-2181, 1994.

[4] D. Blacknell, "Comparison of parameter estimators for K-distribution," *IEE Proc. –Radar, Sonar Navig.*, vol. 141, no. 1, Feb. 1994.

[5] S. Webb, *The Physics of Medical Imaging*, The Bath Press, Avon, Great Britain, 1990.

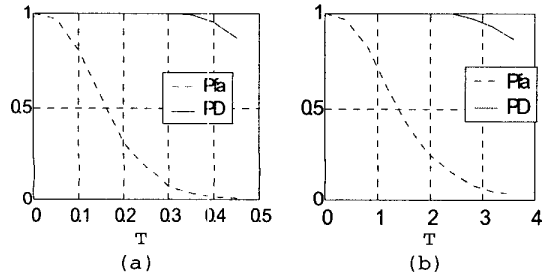

Fig.1. CFAR processor performance, (a): CA- processor for N=6, L=16, SCR=10dB, $V = 1.5$; (b): OS-CFAR processor for k=2, N=6, L=16, SCR=10dB, $V = 1.5$.

Fig.2 Ultrasound image of prostate

(a) (b)

Fig.3(a) An axial detection subregion; (b) a lateral detection subregion.

(a) (b)

Fig.4. Filtered images using (a) orientation-sensitive morphology and (b) conventional morphological filters.

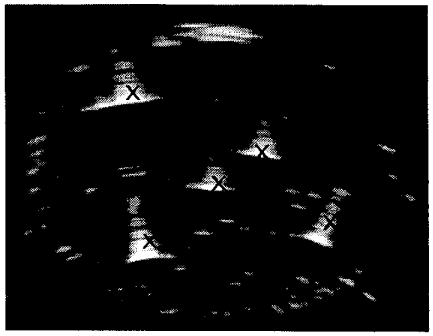

Fig.5. Detection results in which each seed is marked by an X.

Table I: Experimental performance for seed detection.

Exp. #	# Seeds Detected	Actual # Seeds	# False Detect	# Missed Detect	MAE (mm)
1	3	3	1	1	0.92
2	3	3	0	0	0.92
3	4	4	0	0	1.2
4	6	5	1	0	1.16
5	5	5	1	1	0.9
6	6	5	1	0	0.9
7	6	5	1	0	1.12
8	5	5	0	0	1.4
9	4	5	0	1	1.42
10	5	5	0	0	1.16
11	5	5	0	0	0.84
12	5	5	0	0	0.9
13	5	5	0	0	0.46
14	5	6	0	1	0.3
15	11	9	2	0	2.52
16	7	8	1	2	1.12
17	6	6	0	0	1.68
18	6	6	0	0	0.9
19	5	5	0	0	0.84
20	5	5	0	0	1.42
21	5	5	1	1	1.68
22	5	5	0	0	1.44
23	5	5	0	0	1.44
24	5	5	0	0	1.68
25	6	5	1	0	1.44
26	5	5	1	1	0.28
27	5	5	1	1	0.84
28	3	3	0	0	0.84
29	7	5	3	1	1.04
30	9	8	2	1	1.98
31	6	7	0	1	1.78
32	6	5	1	0	0.56
33	5	5	0	0	0.84
34	5	5	0	0	0.64
35	5	5	0	0	0.46
36	4	4	0	0	1.52
37	4	5	0	1	1.12
38	5	5	0	0	1.52
39	5	5	0	0	1.44
40	5	5	0	0	0.9